Chemical Engineering Journal 402 (2020) 126250

Contents lists available at ScienceDirect

Chemical Engineering Journal

journal homepage: www.elsevier.com/locate/cej

From analysis to decision: Revision of a multifactorial model for the *in situ* assessment of NO_x abatement effectiveness of photocatalytic pavements

R. Hingorani*, E. Jimenez-Relinque, M. Grande, A. Castillo, R. Nevshupa, M. Castellote

Spanish National Research Council, Eduardo Torroja Institute for Construction Science (IETcc-CSIC), Madrid, Spain

HIGHLIGHTS

- *In-situ* testing of NO_x abatement of different photocatalytic pavements.
- Robust multifactorial model for predicting photocatalytic effectiveness.
- Knowledge-based decision tool for appropriate photocatalytic material selection.
- Location-dependant variations of NO_x abatement traced back to substrate humidity.
- Carbonation and spalling are significant degradation effects of photocatalytic coatings.

GRAPHICAL ABSTRACT

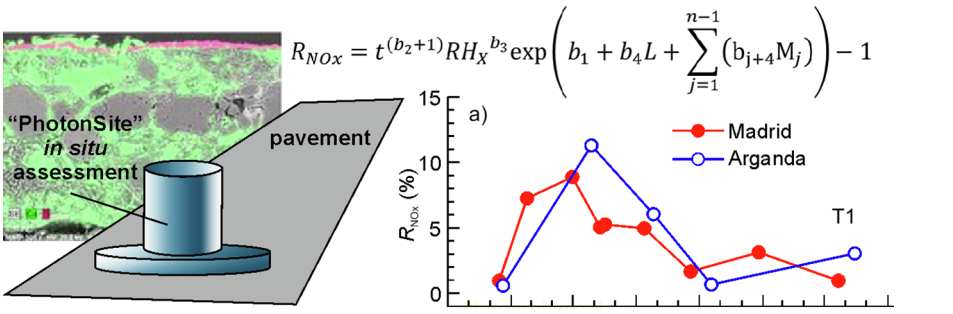

ARTICLE INFO

Keywords:
NO_x abatement
Photocatalysis
Pavement
Environmental variables
Statistical modelling

ABSTRACT

The analysis of NO_x abatement of photocatalytic construction materials under outdoor exposure still presents important challenges. Statistical models are a necessary tool to account for the large uncertainties involved in such complex, multifactorial processes, especially if employed in the context of decision problems confronting local authorities and other stakeholders in everyday practice.

On this background, the paper reports on the revision of a preliminary multiple linear regression model for the comparative study of NO_x removal behavior of urban pavement materials. The model is based on in-situ measurements at pilot plant scale, performed on nine different of such materials. Important advances of the model development include the significant enhancement of its statistical robustness and application boundaries regarding environmental exposure conditions or the materials analysed. The model identifies the material substrate humidity as a key variable and reveals the importance of Ti coating quality. Microscopic characterizations lean support to the model predictions.

1. Introduction

Despite significant efforts made by the governments and key stakeholders pursuing a radical shift of the urban transportation paradigm towards electric mobility, the analytic reports predict that the vehicles with combustion engines including diesel engines will remain the base of the local transport till 2040–2050 [31]. Hence, the problem of urban air contamination by the road vehicle exhaust will persist in midterm that urges to find efficient technologies for its remediation. Apart from the continuous improving of the combustion engines and the search for alternative eco-friendly fuels, photocatalytic nitrogen oxide (NO_x) degradation has been reckoned as one of the promising and cost-effective solutions targeting the urban air decontamination. Considering the kinetic limitations related to very low mean concentrations of NO_x in

* Corresponding author.
E-mail address: hingorani@ietcc.csic.es (R. Hingorani).

https://doi.org/10.1016/j.cej.2020.126250
Received 24 April 2020; Received in revised form 22 June 2020; Accepted 9 July 2020
Available online 15 July 2020
1385-8947/

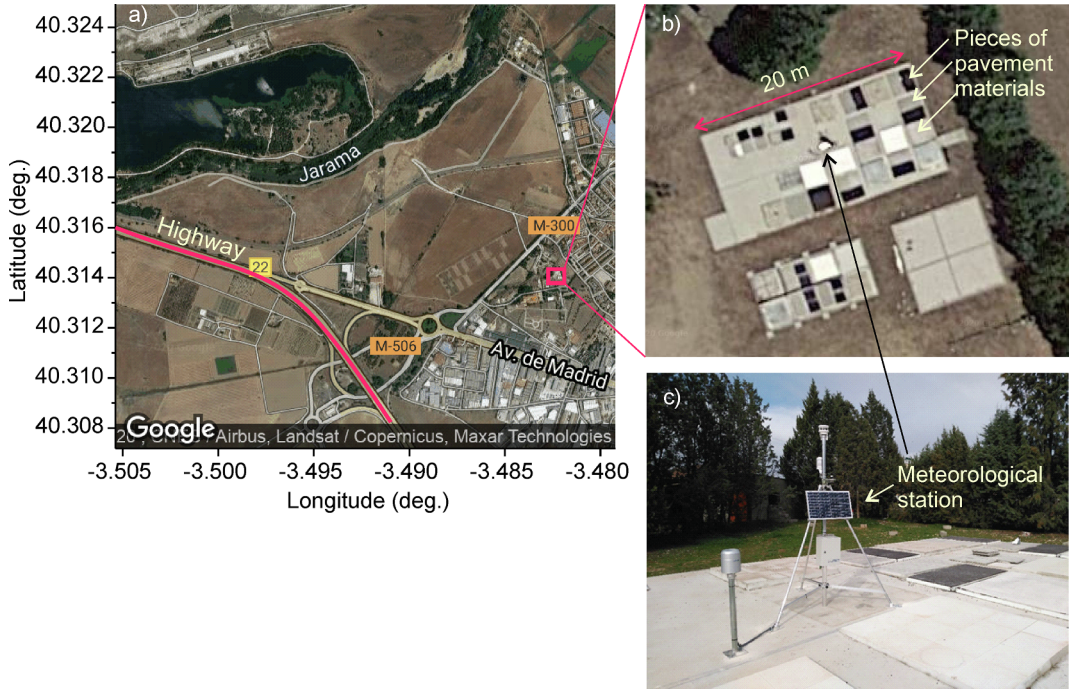

Fig. 1. a) Location of the second pilot scale platform in Arganda; b) satellite image of the bank of proofs at the pilot scale platform; c) photograph of the bank of proofs.

urban air, which are typically below 100 ppb, the effectiveness of the photocatalytic process can be enhanced by placing the photocatalytic material close to the exhaust, e.g. at the road pavement. During the last decade extensive studies have been undertaken to assess the performance of various types of photocatalytic pavement materials using laboratory scale experimental and simulation approaches [1,2,8,11,13,16,18,20–22,27,28]. Some studies scaled up and tested in full-scale pilot projects which were focused on evaluation of the performance of photocatalytic pavements on urban streets under real world conditions [1,3–5,7,9,14,15,24,25,30,32,33]. However, the experimental findings showed large dispersion and were not conclusive. This might be associated with the lack of a standard procedure for measuring the effectiveness of photocatalytic decontamination in real urban environment and the insufficient control of environmental and operational variables [26]. Furthermore, various researchers highlighted significant discrepancies between the simulation results and the real photocatalytic performance of the pavements in urban environment, when the models were fed by the data obtained under well-controlled laboratory conditions [4,12,23].

To tackle this problem a new experimental setup called “PhotonSite” intended to measure the photocatalytic activity of a pavement *in situ* and under real conditions was developed and patented (PCT/ES2016/070808 [6]. The data obtained by “PhotonSite” were validated through the comparison with the results of a standard laboratory test according to ISO 22197:1-2007 [19]. This development paved the way towards the systematic investigation into the influence of environmental variables, seasonal variations, ageing, wearing, weathering and so on upon the photocatalytic activity of various classes of pavements. Such investigation was undertaken in the recently concluded LIFE-PHOTOSCALING project (http://www.life-photoscaling.eu/), in which different photocatalytic materials belonging to three different types were exposed during 17 months to outdoor conditions on pilot scale platforms and monitored. Based on the data obtained at a specific location in Madrid city (Spain), regression models based on simple linear functions were developed, which explain the NO_x reduction effectiveness of the different materials by several explanatory variables, including the exposure time and the hygrometric condition of the material substrate [19]. However, the scope of application of these preliminary models was limited to the analysis of material behavior. Significant drawbacks impede them to be applied in the context of decision-making problems, which the local authorities and other stakeholders face in everyday practice. A strong limitation is that their prediction capacity is limited to the performance of particular commercial products applied to specific substrates under specific urban environmental exposure conditions in Madrid city. In this regard, the previous models lack necessary universality. The fact that they were based on very few observations also calls into question their statistical robustness. The development of a more general model for a comparative analysis of photocatalytic behavior of different materials under various environments would be a significant step forward to a broader employment of this technology, enabling knowledge based decision making in selection of the most appropriate material for each specific location and use conditions.

In this context, further efforts have been made to incorporate additional field data on the photocatalytic effectiveness of the pavements into the study. The data stem from the measurements performed on the second pilot scale platform, at Arganda del Rey town in the Madrid region, hereinafter referred to as Arganda. It is located at about 25 km distance from the centre of Madrid city in the lowland of river Jarama (Fig. 1a) and characterized by a semi-rural environment with a comparatively high relative humidity. The acquisition of the additional field data on the Arganda platforms formed a solid ground for revisiting the existing models, enhancing both their statistical robustness and their scope of application to a wider range of environmental exposure conditions. In addition, the model formulations were redefined in an attempt to extend their application boundaries with regard to the material analyzed. Statistically robust joint formulations for materials corresponding to a specific material type were deduced that consider product-specific influences related to the characteristics of the photocatalyst and its interaction with the substrate, e.g. in terms of the coating quality. Data relevant to explaining such product-specific influences and their degradation with increasing exposure time of the materials (ageing effect) were obtained through experimental characterization of the samples using Scanning Electron Microscope (SEM)

and Back-Scattered Electron (BSE) detector with an Energy Dispersive X-Ray (EDX) analyzer.

2. Experimental

Nine materials belonging to three different types were analysed in the present study. "Material" refers here to the combination of a specific commercial TiO_2-based photocatalytic product applied to a certain type of substrate, distinguished into an open-graded asphalt (24.6% of air voids as determined according to UNE-EN 12697-08:2008) or pavement cementitious tiles. The materials types were the following:

I. Asphalt substrate coated with two photocatalytic slurries (S/A-1 and S/A-2)
II. Cementitious tiles with emulsions containing suspended photocatalytic nanoparticles applied on the surface or spread in the bulk (T-1, T-2, T-3, T-4).
III. Asphalt substrate coated with emulsions containing suspended photocatalytic nanoparticles (E/A-1, E/A-2, E/A-3).

The composition and characteristics of the photocatalysts cannot be disclosed for confidentiality reasons. However, this does not devalue the impact of this study, since the end users targeted will usually not have this information available due to the same confidentiality reasons (see also section 4.3).

As in case of the first pilot scale platform installed in Madrid city, the materials of the second platform were implemented between October and November 2016 in different banks of proofs (BoP) in Arganda (Fig. 1) following the instructions of the manufacturers. More details on the characteristics and the layout of the BoP can be found in [10]. While the first pilot scale platform was situated at a close distance to the M-30 Madrid city highway in a highly stressed urban environment, the second one was located in a semi-urban environment with a considerably lower contamination level and notably higher relative humidity due to the proximity of the Jarama river and wetlands (Fig. 1). The meteorological data including relative air humidity, air temperature, sun irradiation, rainfall intensity, wind velocity and direction and so on were continuously monitored by means of weather stations installed at each platform (Fig. 1).

The NO_x removal effectiveness of the photocatalytic pavements exposed to outdoor conditions was assessed by means of the PhotonSite reactor (Fig. 2). The main advantage of this method is that the measurements can be carried out on the pavement *in situ* without the need of core extraction. The reactor can be used in connection with gas bottles (single configuration) or with outdoor air (double configuration). It is equipped with a UV or visible light irradiation system, which can be substituted by direct sunlight irradiation through a transparent viewport. A stainless steel cover is applied on the viewport, when using internal light sources. Temperature and relative air humidity inside the chamber are also monitored during the test. The latter can be considered a constant ($RH_{int} \approx 25\%$).

Fig. 2a shows the layout of the equipment at a BoP during the PhotonSite test. The reactor was used in single configuration. Two mass flow controllers were used to introduce the NO_x/air mixture with NO concentration of 450 ± 50 ppb_v and 20 ± 5 ppb_v of NO_2 with a gas flow rate of 3 l min^{-1} into the reactor chamber situated on the top of the pavement surface subjected to the test. The chamber flange being in contact with a pavement area of 176.7 cm^2 was properly sealed to avoid gas leakage (Fig. 2b). A fan then homogenized the NO_x concentration inside the reactor, which was monitored using a chemiluminescence analyzer (AC-32 M, Environment S.A.). After the NO_x concentration in the chamber stabilized, the pavement inside the chamber was irradiated

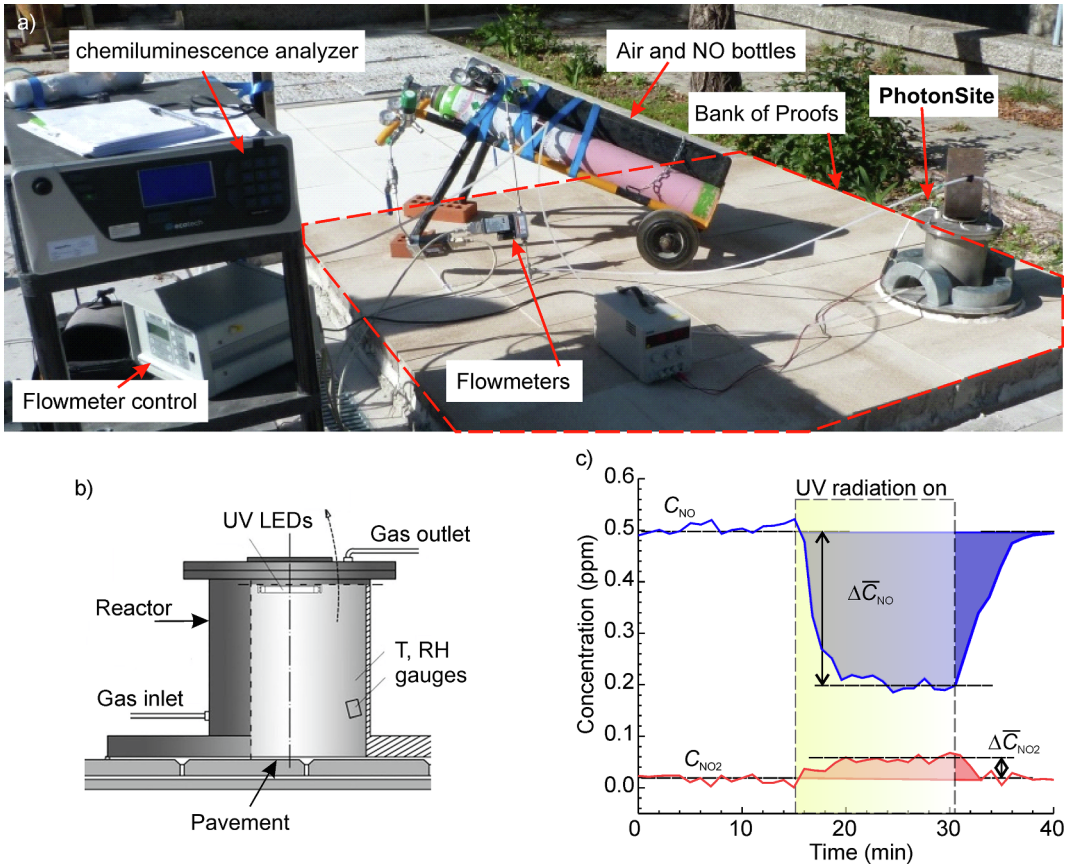

Fig. 2. a) Layout of the experimental setup for *in situ* measuring of NO_x removal effectiveness on a bank of proofs; b) schematic drawing of PhotonSite reactor; c) representative time series of NO and NO_2 concentrations during the *in situ* PhotonSite test.

for t_{irr} = 15 min using five light emitting diodes (LedEngin UV 365 nm, 5w (0.5w) LZ1U605 Bin U 115°) with an irradiance of 10 Wm^{-2}. The photocatalytic activity of the material was determined from the NO and NO_2 concentration time series (Fig. 2c), recorded by a data acquisition system.

The NO_x removal effectiveness R_{NOx} was defined as a percentage of NO_x concentration that is abated by the photocatalytic pavement during the test. It is determined according to eq. (1), where ΔC_{NO} is the amount of NO concentration (ppb) removed and ΔC_{NO2} is the amount of NO_2 concentration formed during time t_{irr} (Fig. 2c). C_{NOx} is the initial concentration of NO_x (NO + NO_2) before onset of irradiation. To make the results comparable with whose obtained through the standard ISO 221971:1, normalization of the reaction surface S in the test (176.7 cm^2) to the nominal surface of the standard ISO 22197:1 (49.25 cm^2), SN, was carried out.

$$R_{NOX} = \frac{\int \Delta_{C_{NO}} dt_{irr} - \int \Delta_{C_{NO_2}} (dt_{irr}) \frac{SN}{S}}{C_{NOX}} \cdot 100 \quad (1)$$

Between February 2017 and June 2018, fourteen PhotonSite measurements were performed on each slab of the nine materials selected for this study. Out of these, nine measurements correspond to the 1st platform (Madrid) and the other five to the 2nd platform (Arganda). After three and nine months of outdoor exposure, cores were extracted from the slabs by dry cutting and examined by SEM and BSE with simultaneous EDX analysis.

3. Results

3.1. PhotonSite measurements

The experimental results of the 17 month-long *in situ* measurements on nine pavement materials at the two pilot scale platforms are shown in Figs. 3, 4 and 5. The type I pavement materials (S/A) showed a well-defined seasonal variation of the R_{NOx} with maxima and minima corresponding to spring-summer and autumn–winter periods, respectively (Fig. 3). It should be highlighted that in most cases the second maximum was close in intensity to the first one despite a one-year time span between them. In the intermediate autumn–winter period a significant performance loss, as high as 50% of the corresponding maxima, could be noticed.

For the type II materials (T) the seasonal variation was less pronounced (Fig. 4) than for type I, but with larger variation in amplitude. However, there is certain parallelism between the type I and II, since both yielded maximum photocatalytic effectiveness during warm and dry periods, while during cold and damp seasons their photocatalytic effectiveness significantly decreased. In similarity to the type I materials, most of the tested tiles (T-4, T-3 and T-2 in Arganda) exhibited a

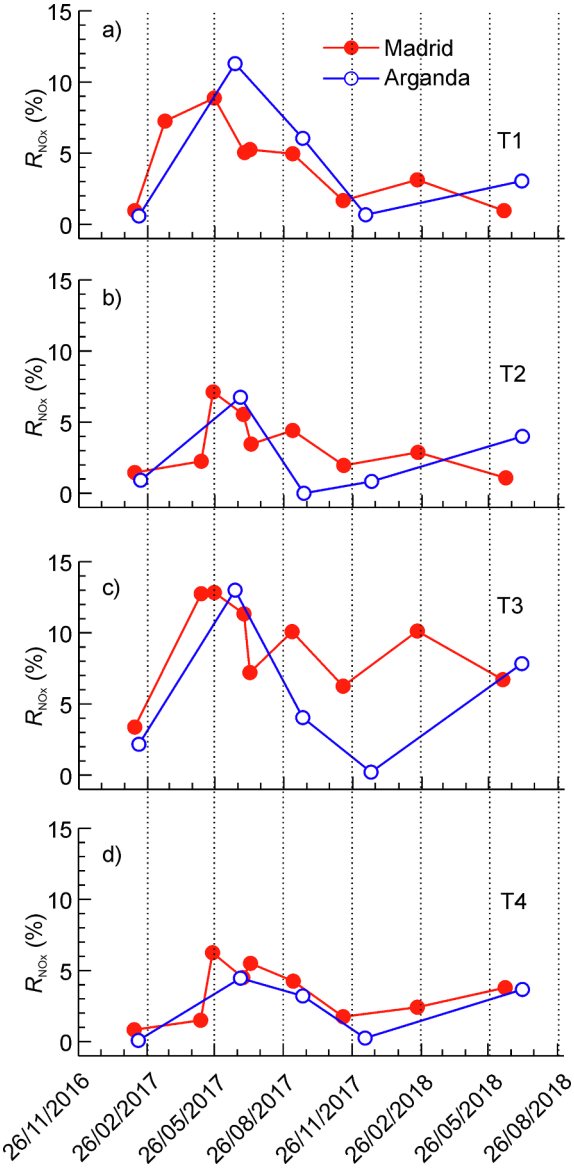

Fig. 4. NO_x removal efficiency R_{NOx} as obtained in measurements between February 2017 and July 2018 on T materials (type II) located in Madrid and Arganda.

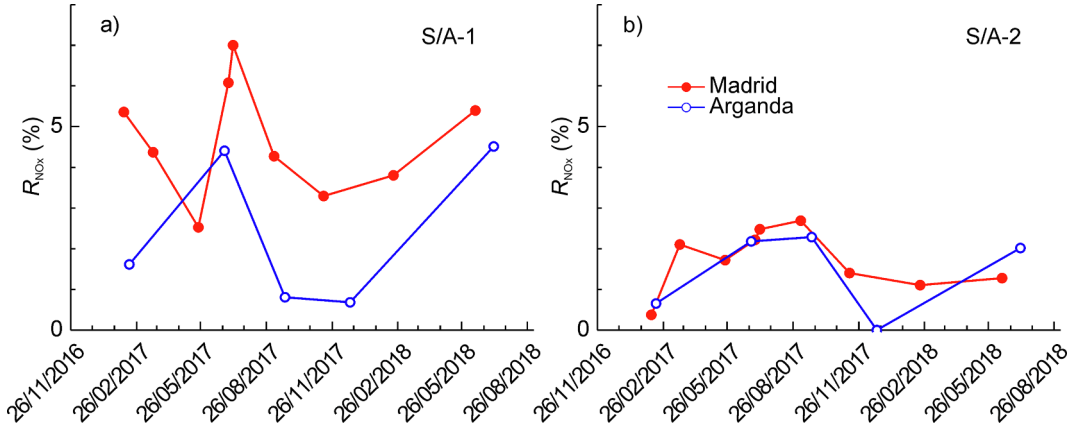

Fig. 3. NO_x removal efficiency R_{NOx} as obtained in measurements between February 2017 and July 2018 on S/A materials (type I) located in Madrid and Arganda.

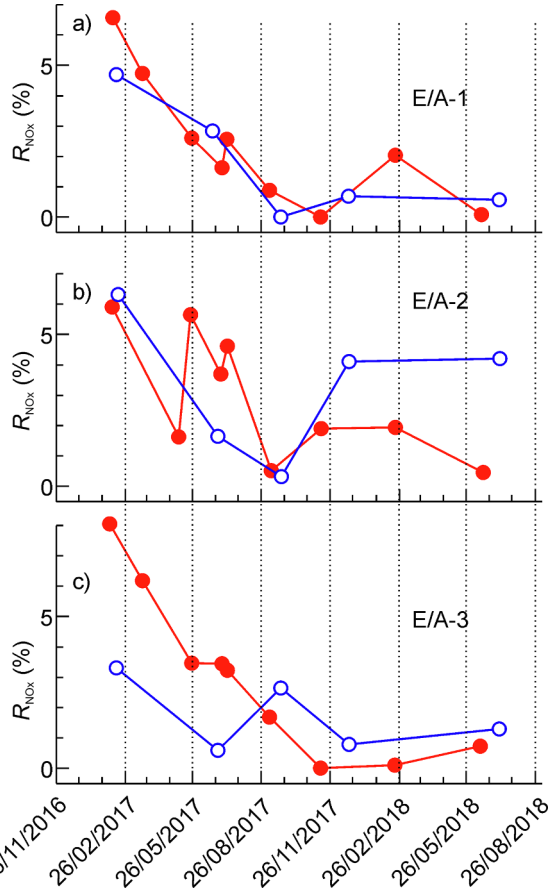

Fig. 5. NO_x removal efficiency R_{NOx} as obtained in measurements between February 2017 and July 2018 on E/A materials (type III) located in Madrid and Arganda.

significant recovery of the photocatalytic effectiveness after the preceding winter season.

In contrast to type I and II, the type III materials (E/A) showed a gradually decreasing tendency with very weak oscillations (Fig. 5), suggesting that the R_{NOx} behaviour was controlled by ageing rather than by meteorological conditions.

Apart from the behavioural dissimilarities, the photocatalytic effectiveness were subjected to significant quantitative variability between different material types. The Kruskal-Wallis test being a non-parametric alternative to the conventional one-way Anova test was used for testing this hypothesis. Applied to the R_{NOx} measurements performed at both platforms ($N = 126$ observations) of the three material types studied (degrees of freedom (DoF) = 2), the test delivered the p-value 0.012, suggesting that the three samples originate from different populations. The largest sample mean $\bar{R}_{NOx}$ corresponded to the type II materials (Table 1) what highlights the significant influence of the substrate material. Indeed, three out four materials belonging to type II (T) differ from the type III materials (E/A) only by the type of substrate: cementitious tiles (type II) vs. open-graded asphalt (type III).

In addition to the substrate type, the R_{NOx} was influenced by the photocatalytic product-specific characteristics. This was especially significant in case of the type I and II materials. The differences between the populations for S/A-1 and S/A-2 materials were statistically significant according to the Kruskal-Wallis test performed ($N = 28$, $DoF = 1$, $p = 0.002$). Similar conclusion were drawn for the four studied materials of type II ($N = 56$, $DoF = 3$, $p = 0.008$). In contrast, the differences between the populations of the three type III materials were not statistically significant ($N = 42$, $DoF = 2$, $p = 0.49$).

Figs. 3 to 5 show a generally similar behaviour of the materials on both pilot scale platforms. This observation is underpinned by the Kruskal-Wallis tests, which compared the R_{NOx} data obtained for same materials situated in Madrid and Arganda. The null hypothesis that the Madrid and Arganda samples correspond to the same population could not be rejected ($N = 14$, $DoF = 1$, $p > 0.05$). However, on closer inspection of Figs. 3 and 4, significant quantitative differences between both platforms can be observed for some materials (S/A-1, S/A-2, T-3), specifically during the winter season, when R_{NOx} measured in Arganda dropped to insignificant values (in some cases even to zero), while in Madrid the materials remain active, although with low R_{NOx}. Such a different behaviour is also inferable from Table 1, which shows for most materials a comparatively better average performance in Madrid. This finding can be associated to location-dependant environmental conditions, as will be further discussed below in Sections 3.2 and 4.

3.2. Influence of environmental variables

In the previous section it was shown that the photocatalytic performance of the S/A and T materials (Figs. 3 and 4) was higher during warmer and dryer periods of the year. This *season-dependant behaviour* is indicative of the influence of environmental variables on the R_{NOx}. The outdoor air relative humidity (RH) was immediately excluded from these variables, since during the "PhotonSite" test RH was imposed by the gas inlet process (section 2) and maintained constant inside the reactor ($\approx$25%). Hence, the ambient air RH during the test was irrelevant to the measured data. The same can be applied to the irradiance (W), which was also controlled in the "PhotonSite" test ($\approx$10 Wm^{-2}). The temperature inside the reactor can be approximated by a linear function of the outdoor temperature during the tests and might, hence, contribute to the explanation of seasonal variations of the measured R_{NOx}. However, the previous analysis provided no statistical evidence to this end for most of the studied materials [19]. The previous results suggested that the seasonal variations of the NO_x removal effectiveness could be mainly attributed to the humidity of the material substrate, RH_{sub}. The present study based on the comparative analysis of the data obtained at two different locations revealed that RH_{sub} can likewise explain the *location-dependant differences* in R_{NOx} (see section 3.1).

Fig. 6a shows the relative humidity, RH, measured by means of meteorological stations situated on the test platforms in Madrid and Arganda during December 2017. It can be observed that the daily minima at both locations are almost equal. On the contrary, the daily maxima were substantially higher in Arganda during large part of the month. This observation seems to provide a direct explanation for the fact that during the winter season some of the S/A and T materials exposed in Madrid perform significantly better than in Arganda (Figs. 3 and 4). However, some additional explanations are required in order to understand the role of RH on R_{NOx}. While instantaneous RH had no influence on the R_{NOx} measurement, on a larger time scale it can be linked to the general hygroscopic conditions of the materials, e.g. the

Table 1
Average $\bar{R}_{NOx}$ (%) for materials tested in Madrid, Arganda and the total for both pilot scale platforms.

Location	Number of tests	S/A-1	S/A-2	E/A-1	E/A-2	E/A-3	T-1	T-2	T-3	T-4
Madrid	9	4.7	1.7	2.3	2.9	3.0	4.2	3.3	9.0	3.4
Arganda	5	2.4	1.4	1.8	3.3	1.7	4.3	2.5	5.4	2.3
Both	14	3.9	1.6	2.1	3.1	2.5	4.3	3.0	7.7	3.0

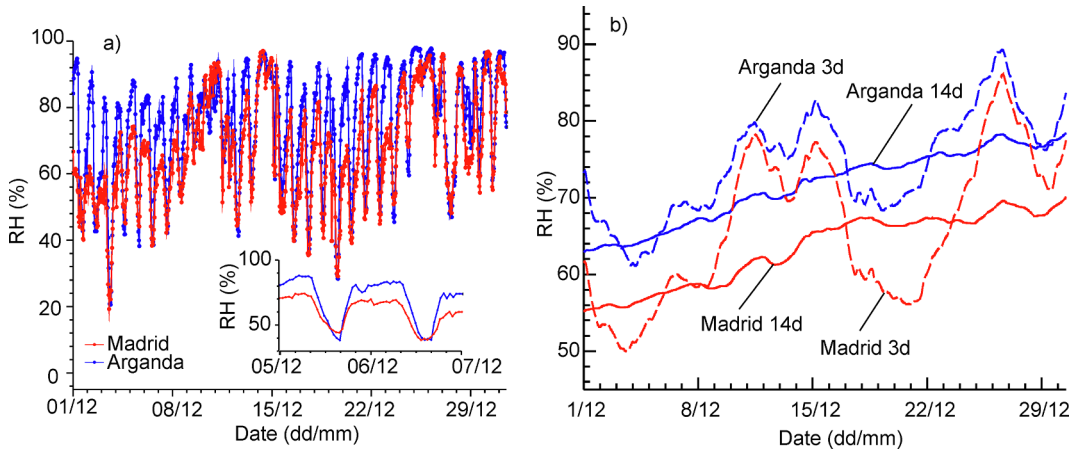

Fig. 6. a) Time series of measured outdoor relative humidity as obtained by meteorological stations situated on the test platforms in Madrid and Arganda during December 2017. The inset shows the enlarged view of the data variation during two days; (b) moving average of the time series shown in graph a) with averaging period of $X = 3$ and 14 days preceding the PhotonSite test.

humidity of the material substrate, RH_{sub}. The question arises about the time scale on which the air RH correlates with the material substrate humidity. Due to the hygroscopic inertia of construction materials (Baroghel-Bouny, 2007), the water adsorption and desorption mechanisms cannot immediately respond to significant variations of RH within a time span of only a few hours (Fig. 6a). Hence, a priori, the sought time scale spans from several days to several weeks. In case the correlation between the substrate and the air humidity is confirmed on a certain time scale, the average of air RH over the characteristic period of time immediately preceding the "PhotonSite" measurement can be used as a model variable to characterize the hygroscopic conditions of the material during the test. This approach, introduced in [19], becomes intuitively clear upon inspection of Fig. 6b, which shows the average relative humidity, RH_X, where X specifies the number of days over which the air humidity should be averaged, covering a reference period of, respectively, $X = 3$ and $X = 14$ days. Generally, the larger the reference period X, the smoother the graphs. The value for X that best represents the hygroscopic behaviour of the material substrates was found using statistical analysis (section 4).

4. Discussion

4.1. Statistical model and analysis procedure

In section 3, the main potential influence factors on the NO_x removal efficiencies (R_{NOx}) of the materials analysed by means of the "PhotonSite" device were identified. With the aim to provide further quantitative evidence for these influences, a multiple linear regression analysis was employed. Given the fundamental role of the *material type*, clearly manifested in Figs. 3 to 5 and supported by the result of the Kruskal-Wallis test (section 3.1), three individual data samples were analysed, comprising, respectively, 28 (type I), 56 (type II) and 42 (type III) data points. The regression model that best represents the relationship between the R_{NOx} measured in the "PhotonSite" tests (section 3.1) and different potential explanatory variables X_i, is given by equation (2). The lower case letters b_i stand for the model parameter estimates. The most relevant characteristics considered by the model and the corresponding explanatory variables are listed in Table 2.

Among the potential explanatory variables X_i, the natural logarithm of exposure time t accounts for the *ageing effect* of the materials. The log-transformed average relative air humidity over the last X days before the NO_x removal test, RH_X, considers the influence of the *substrate humidity* RH_{sub} on R_{NOx}, where X was varied between 0 (instantaneous RH), 1, 3, 7, 14 and 28 days. Moreover, the model contains a location (*dummy*) variable L, which distinguishes between the different environmental exposure in Madrid ($L = 1$) and Arganda ($L = 0$), respectively. Finally, the summation term in the model introduces (*dummy*) material variables M_j that account for differences related to the characteristics of the photocatalyst as well as to its interaction with the substrate surface (quality of the Ti layer). In this term, n represents the number of products per material type (I: $n = 2$; II: $n = 4$; III: $n = 3$).

$$\ln((R_{NOx}+1)/t) = b_1 + b_2\ln(t) + b_3\ln(RH_X) + b_4L + \sum_{j=1}^{n-1}(b_{j+4}M_j) \quad (2)$$

It should be stressed that model (2) presents several important modifications with respect to the previous models [19]]. The introduction of L pursues to show that the substrate humidity, considered via RHx, can explain location-dependant environmental influences on R_{NOx} (section 3.2). If solid arguments could be found to support this, the location-dependency could be omitted from the model, thus, considerably extending the degree of the model universality and validating its ability for application in various environments. Another strong improvement of the model concerns the consideration of material-specific influences. While the previous models were limited to predictions for particular commercial products applied to a specific substrate, the present approach accounts for such influences by means of a simple variation of the model constant (vía material variables M_j and the associated parameter estimates b_{j+4}). A clear association of this variation with certain characteristics of the photocatalysts (e.g. grain size, surface area, crystallinity, TiO_2 phases, etc.) and/or its interaction with the

Table 2
Relevant characteristics represented by the different explanatory variables.

Variable	Units	Characteristics	Description
t	Months	Exposure time	Number of months between implementation of the materials at the platform and the NO_x measurement
RH_X	%	Substrate humidity	Relative air humidity over the last X days before the NO_x removal test
L	–	Location dependent influences	Dummy variable accounting for differences due to different exposure conditions at the two platforms (Madrid, Arganda)
M_j	–	Material-related influences	Dummy variables accounting for influences related to the composition of the photocatalytic product as well as to its interaction with the substrate

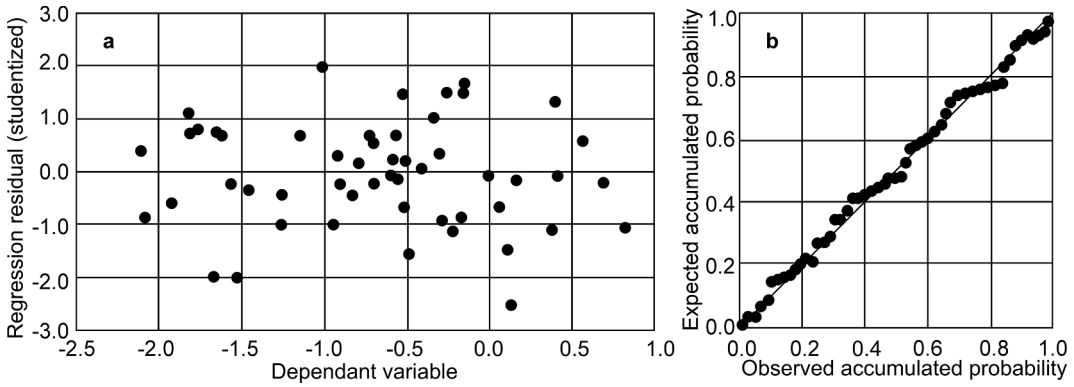

Fig. 7. Studentized residuals versus predicted value (a) and *P-P* plot (b) of model (2), assuming $X = 3$. The model was fed with experimental data for the type II materials (T).

substrate, e.g. in terms of the quality of the Ti layer (continuity, homogeneity, thickness or adhesion), would enhance the utility of the model from a mere analysis instrument to a comparative prediction tool to be used in the context of decision making processes. The discussion will continue in Section 4.2.

A statistical robust formulation is another necessary condition for the use of the model for the purpose of decision analysis. The previous models do not fulfil this condition for they are based on very few observations. This fact also impeded a proper verification of essential requirements to multiple linear regression models. The incorporation of additional data (from the Arganda platform) and the approach of joint formulations for materials corresponding to a specific material type (by introducing material variables M_j) enabled such verifications in the present study. In this sense, the log-transformations in (2) contribute to stabilizing the variance of the regression model error. The normalization of the dependent variable by time variable t also pursues this aim. The diagram relating externally studentized residuals to predicted values confirms homoscedasticity and independency of the model errors (Fig. 7a). Potential outliers were identified as values with externally studentized residuals outside the range $\pm$ 3.0. The *P-P* plot that shows the expected versus the observed accumulated probability (Fig. 7b), supports the validity of the hypothesis of normally distributed residuals.

A stepwise backward elimination analysis was employed to determine the significance of various variables using *t*-test and the significance level $\alpha = 0.05$. Absence of significant multicollinearity between the X_i was verified by controlling the variance inflation factors (VIF). The evaluation and comparison of the goodness-of-fit of the regression models to the experimental results is based on the adjusted coefficient of determination R_a^2, which takes into account the number of degrees of freedom [29].

After resubstituting the log-transformed variables, the regression model (2) can be expressed as follows:

$$R_{NOx} = t^{(b_2+1)} R H_X^{b_3} \exp\left(b_1 + b_4 L + \sum_{j=1}^{n-1} (b_{j+4} M_j)\right) - 1. \quad (3)$$

4.2. Results and discussion

Feeding model (2) with the experimental data of type III materials (E/A), the backward elimination procedure revealed that only the log-transformed time variable t is statistically significant for the explanation of the R_{NOx} variance. In line with the previous findings [19], none of such factors as the substrate humidity, the location or the product specific effects, influence R_{NOx} in a significant manner. The lack of influence of the different products was anticipated by the Kruskal-Wallis test results (Section 3.1).

Table 3 summarizes the parameter estimates b_i for the model constant and time variable ln(t), as well as the associated standard deviations s_{bi}. The corresponding *p*-value provides strong evidence to reject the null hypothesis that the exposure time t does not significantly influence the NO_x removal efficiencies of the type III materials. The quality of the model predicting the NO_x abatement effectiveness was reasonably high as follows from $R_a = 0.82$ (Fig. 8). However, the coefficient of variation for the ratio between the observed and predicted R_{NOx} of the order of 90% indicates the considerable model uncertainties. These uncertainties are also represented by the means of the bounds of the 95% confidence interval for the expected value, $b_{i,95}$, given in Table 3 and plotted in Fig. 8.

Table 3
Parameter estimates b_i and corresponding standard deviation s_{bi}, *p*-value and bounds of the 95% confidence interval $b_{i,95}$ for statistically significant regression model variables (type III materials).

i	Variable	b_i	s_{bi}	*p*-value	$b_{i,95,low}$	$b_{i,95,up}$
1	Constant	2.85	0.30	$< 10^{-4}$	2.25	3.45
2	ln(t)	−1.80	0.13	$< 10^{-4}$	−2.06	−1.54

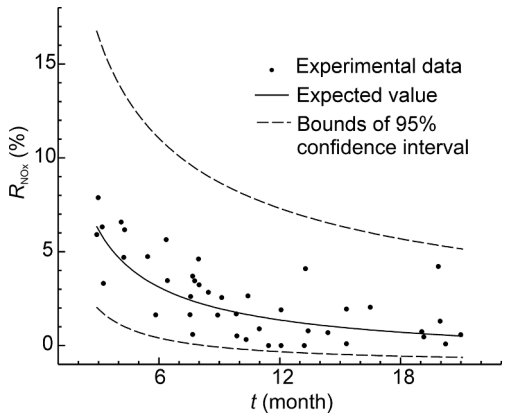

Fig. 8. Observed (dots) and predicted (lines) expected value and bounds of 95% confidence interval for the efficiencies R_{NOx} of type III materials versus time variable t.

The previously described results are in good agreement with the microscopy observations of the E/A samples. Since no Ti could be observed when analysing the asphalt samples by BSE in a transversal cut, their surface was observed by SEM. As a representative example of these materials, Fig. 9 shows the micrographs of material E/A-1 after a) $t = 3$ months and b) after $t = 9$ months of exposure. After three months, the layer was not completely homogeneous showing lack of Ti (in pink) in some areas. However, after nine months, Ti was only scarcely found on the sample surface. These observations suggest a

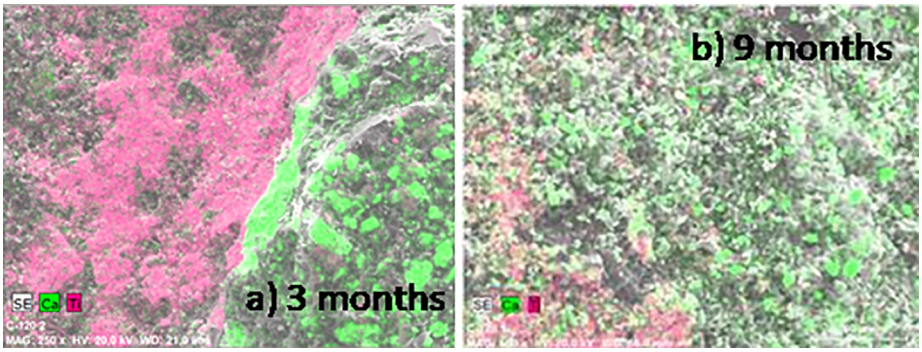

Fig. 9. SEM micrographs of the sample E/A-1 after a) 3 months and b) after 9 months of exposure. (Ti in pink, Ca in green).

generally poor adhesion between the photocatalytic emulsions and the asphalt, which significantly deteriorated with increasing exposure time. This provides a reasonable explanation to the strong time-dependent performance of the type III materials (Fig. 8).

In contrast to the type III materials, for type I and II materials the influence of the average relative humidity RH_X on the explanation of variations in R_{NOx} was statistically significant, in accordance with literature [19]. This finding is valid irrespective of the value X considered in the model. However, a more detailed analysis provides a solid ground for the robust assessment of the influence of substrate humidity on R_{NOx} through the parameters RH_3 or RH_7, as will be shown in the following.

Fig. 10a shows the variation of R_a^2 with the number of days X used to average the air RH. Two qualitatively similar graphs corresponding to, respectively, the type I and II materials can be distinguished. In both cases, the goodness of the model fit generally increases with rising X, up to $X = 14$. Further increase of X to 28 led to decrease the goodness of fit. Especially noticeable is the considerable increase from $X = 0$ to $X = 1$ observed for the tiles (type II), clearly confirming that the instantaneous air humidity RH_0 is irrelevant to the representation of the substrate humidity.

The fact that both graphs shown in Fig. 10a reach maximum at $X = 14$ days suggest that this reference period is the most adequate for determining RH_X. However, as shown before in Fig. 6, the discussion about the influence of RH on R_{NOx} cannot evade an analysis of the location dependency. For this purpose, Fig. 10b shows the p-value corresponding to the location variable L as a function of X. Again, both graphs have a qualitatively similar evolution. For comparatively large X, the location variable L is statistically significant (p-value < 0.05), pointing to a different behaviour in Madrid and Arganda, respectively. However, this not the case if smaller reference periods X are considered. Indeed, for $X \leq 3$, the p-value for both graphs exceeds the threshold value of 0.05. This suggests that relatively short reference periods for averaging RH, i.e. $X = 1$ or $X = 3$, provide suitable measures to capture the location-dependant differences, related to the relatively frequent variations of the humidity of the material substrates. This statement is clearly supported by Fig. 6b, where the difference between the smoothened RH_{14} graphs corresponding to both locations remains approximately constant along the represented period, whereas the difference between the RH_3 graphs varies significantly over time.

Fig. 10b reveals that, when imposing a more stringent requirement to statistical significance of an independent variable, for instance the frequently used p-value $= 0.01$, the reference periods X of up to approximately seven days would turn out to be suitable for representing the hygrometric conditions of the substrate values. Given the comparatively worse model fit for $X = 1$ (Fig. 10a), the adoption of the minimum value $X = 3$ is recommended when choosing the optimum, consistent with previous findings [19]. In the range $3 \leq X \leq 7$, the goodness of the model, characterized by constant R_a^2 of 0.84 and 0.82, corresponding to the S/A and T materials, respectively, is not affected (Fig. 10a). In summary, periods between $X = 3$ and 7 days present an adequate trade-off between the location-sensitivity and the goodness of fit.

Table 4 summarizes the results of the regression analysis conducted for the type I (S/A) and type II (T) materials, assuming the material substrate humidity to be adequately represented by RH_3. As discussed above, in this case, the location variable L is being eliminated during the backward elimination procedure ($b_4 = 0$). The negative parameter estimates b_2 and b_3 indicate that, as could be expected, both RH_3 and exposure time t, have a negative influence on the NO_x efficiencies of the materials, i.e. the larger RH_3 or t, the smaller is their pollutant degradation efficacy R_{NOx}. In contrast to the findings for the type III (E/A) materials, where t was found to be the only significant influence variable on the efficiencies (Fig. 8), the substrate humidity, represented by

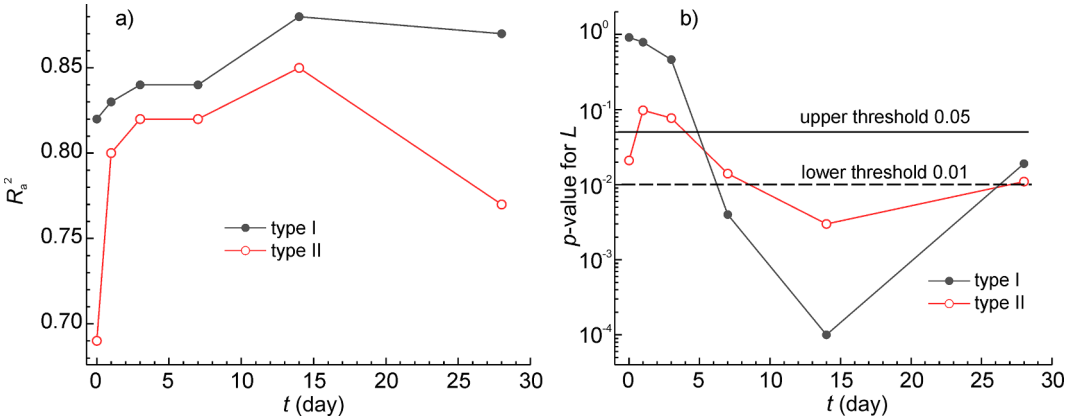

Fig. 10. a) Adjusted R^2 and b) p-value for location variable L versus number of days X assumed for computing average relative humidity, RH_X (the threshold values 0.05 and 0.01 are shown by dashed and continuous lines, correspondingly).

Table 4
Parameter estimates b_i and corresponding standard deviation s_{bi}, p-value, bounds of the 95% confidence interval $b_{i,95}$ and Variance Inflation Factor (VIF) for statistically significant regression model variables (S/A and T materials).

i	Variable	S/A (type I)						T (type II)					
		b_i	s_{bi}	p-value	$b_{i,95,low}$	$b_{i,95,up}$	VIF	b_i	s_{bi}	p-value	$b_{i,95,low}$	$b_{i,95,up}$	VIF
1	Const.	4.67	1.00	$< 10^{-4}$	2.61	6.73	–	7.38	0.72	$< 10^{-4}$	5.93	8.84	–
2	ln(t)	−1.05	0.11	$< 10^{-4}$	−1.28	−0.82	1.10	−1.14	0.09	$< 10^{-4}$	−1.33	−0.95	1.15
3	ln(RH_3)	−0.94	0.23	4×10^{-4}	−1.42	−0.47	1.10	−1.49	0.16	$< 10^{-4}$	−1.81	−1.17	1.14
5	M_1	0.67	0.12	$< 10^{-4}$	0.41	0.92	1.00	0.74	0.11	$< 10^{-4}$	0.52	0.97	1.01

RH_3, governs the NO_x removal behaviour of the S/A and T materials. On the contrary, the exposure time t has a comparatively small influence on R_{NOx}. This can be well observed in Fig. 11, which depicts the expected value for R_{NOx} according to (3), as a function of RH_3 and different values of t.

Fig. 11 further reveals product-specific differences among the type I and II materials, as already suggested by the Kruskal-Wallis test (section 3.1). Fig. 11a shows that the model attests a significantly better performance for S/A-1 than for S/A-2. Similarly, the model predicts T-3 to remove more than twice the amount of NO_x than, respectively, T-1, T-2 and T-4 (Fig. 11b).

In any case, Fig. 11 shows that the obtained regression models are subject to significant uncertainties and require further improvements. A proof of these uncertainties are the relatively large coefficients of variation CoV of the ratio between observed and predicted R_{NOx}, which amounts to about 40–50% depending on the material type considered ($CoV_{S/A} = 0.39$; $CoV_T = 0.47$).

The detected difference in the behaviour between materials of the same type (I, II), considered by the dummy variable M_j, may be related to various characteristics of the photocatalyst such as grain size, surface area, crystallinity, TiO_2 phases, presence of defects or dopants, etc., which could not be included in the analysis due to the limitations imposed by the product manufacturers via the underlying confidentiality agreements. Furthermore, this difference can be related to the Ti coating quality in terms of continuity, homogeneity, thickness or adhesion to the substrate surface. If these factors are relevant from the beginning of the material exposure ($t = 0$), such influences should be considered by the explanatory variable M_j. On the other hand, if the defects appear during the service life ($t > 0$) they are taken into account by the ageing variable t, as previously discussed for the type III materials (Fig. 9).

Furthermore, chemical reactions can occur between specific substrates and the environment leading to the alteration of the photocatalytic effectiveness of the materials. A relevant example is carbonation, the reaction between the $Ca(OH)_2$ of cement and the atmospheric CO_2 to form calcite ($CaCO_3$). The latter can block the access of NO_x to the TiO_2 active centres and shadow the surface from UV radiation. This gradually reduces the effectiveness with time. The carbonation reaction only occurs in cementitious materials belonging to types I and II, but not the type III.

Fig. 12 shows BSE micrographs of the cross-sections of two samples: a) T-1 and b) T-3 after three and nine months of exposure. In the former, it is shown that a significant part of Ti has been penetrated into the matrix of material T-1, where it is not subjected to UV radiation and, therefore, does not participate in the photocatalytic processes. The photocatalytic layer on T-1 is discontinuous, inhomogeneous and thinner than in case of material T-3. The coating on T-3 is well adhered to various components of the substrate. Thus, it can be concluded that the active coatings on T-1 and T-3 are significantly different from the beginning of the test ($t = 0$). This in in accordance with the results of the statistical analysis, which showed, via variable M_j, that material T-3 performed significantly better, than the other tiles tested (Fig. 11b).

In Fig. 12 it can be further observed that after nine months' outdoors exposure, the Ti layer of material T-1 has experienced significant deterioration probably due to a gradual spalling and weathering related to insufficient adhesion strength. This observation is in agreement with the time-dependant decrease of the T-1 material effectiveness (Fig. 4), clearly reflected in the model via the ageing variable t (Fig. 11b).

The situation is different for material T-3, where a compact Ti layer maintained on the surface after nine-month exposure (Fig. 12). In this case, the time-dependant decrease of R_{NOx} (Fig. 4), predicted by the regression model via t (Fig. 11b) cannot be attributed to loss of adherence. In case of T-3, the decrease of R_{NOx} with time has to be attributed to carbonation. The chemical mapping of the surface (Fig. 13) shows that the compact layer of TiO_2 is partly covered with crystals of $CaCO_3$, an effect that reduces the photocatalytic performance of the material.

4.3. Final considerations

The average NO_x abatement effectiveness measured in this study is far lower in comparison with the measurements carried out using AQ

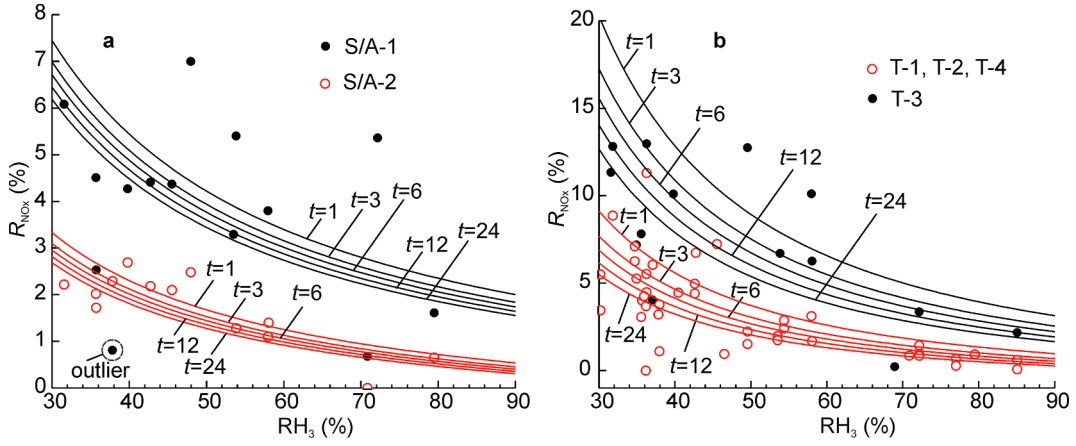

Fig. 11. Observed (dots) and predicted (lines) expected value for the R_{NOx} as a function of average relative humidity RH_3 and time variable t: a) Type I; b) Type II.

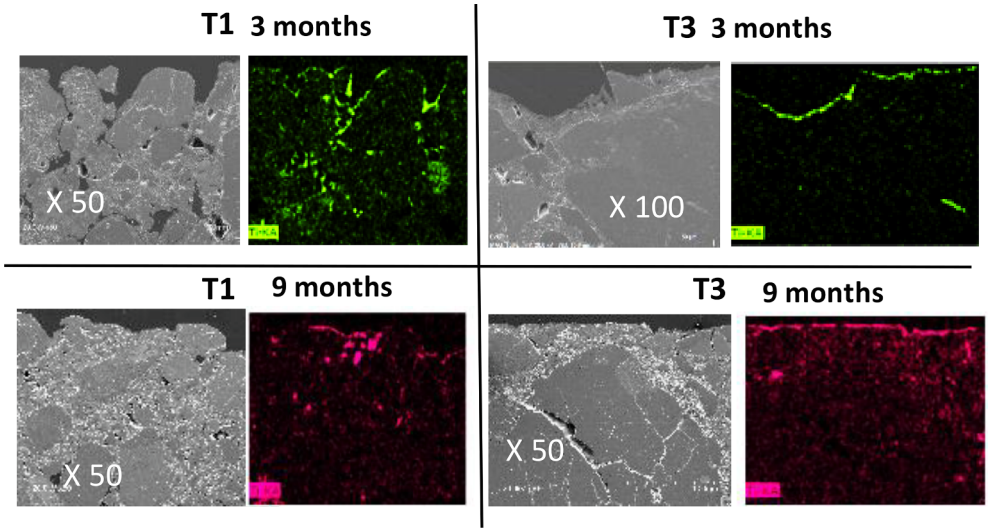

Fig. 12. BSE micrographs of T-1 (a) and T-3 (b) after 3 and 9 months of outdoor exposure. Ti maps are shown in green (3 months) and magenta (9 months).

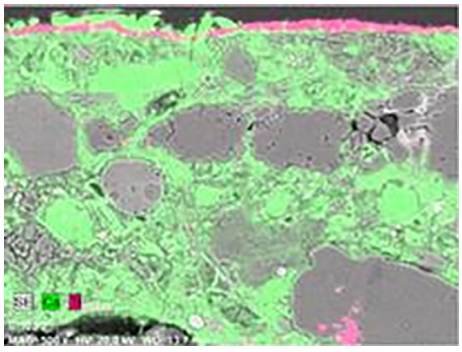

Fig. 13. BSE micrograph (×500) of T-3 after 9 months of outdoor exposure. Ti – magenta, Ca - green.

mesh low-cost sensors, which occasionally yielded the values as high as 75% [10]. However, the mentioned study was performed under real world pollutant concentrations in the air at the ground level, which was around few tens of ppb, while in the present study the NO concentration was approximately ten-fold higher, about 450 ppb (section 2). Previous studies including [10] suggested that the NO_x abatement effectiveness increases with decreasing the NO concentration, hence explaining the far lower removal efficiencies obtained in the "PhotonSite" tests. Another drawback of these tests is related to the constant air RH inside the reactor (section 2). Previous studies showed that instant air humidity can have certain influence upon the photocatalytic NO_x abatement effectiveness, see e.g. [10]. Such a short-term effect of RH could not be analysed in the present study, which focusses on the influence of the long-term component (RH_X).

The "PhotonSite" test procedure endeavours to strike a balance between the degree of realism and the practical usefulness of the method in terms of costs and time consumption. Further modifications to the test procedure can be considered in the future pursuing better simulation of real-world environmental conditions. In spite of the current drawbacks of the "PhotonSite" test, the derived statistical models constitute a powerful tool for they shed light onto the most relevant processes responsible for the performance and degradation of various photocatalytic pavement materials. In addition, the models can provide support to decisions concerning the appropriate choice of photocatalytic pavements in practical applications, provided the modelling results are used for comparative purposes only.

Another prerequisite for employing the models as a decision tool, is that specific materials belonging to the S/A or T type (not relevant for E/A materials) can be previously associated with one of the two performance levels the model distinguishes through changes of the model constant (via dummy variable M_j and associated parameter estimate b_{j+4}), as illustrated in Fig. 11. As discussed under section 4.2, the two performance levels could be associated with certain characteristics defining the quality of the Ti layer, e.g. its homogeneity, continuity or adhesion to the substrate (Fig. 12). In addition to microscopy observations performed here, such characteristics might be quantified based on simple laboratorytests such as those described in [31].

Further improvements of the models could address a more refined representation of material-related influences. In particular, the characteristics of the photocatalyst (grain size, surface area, crystallinity, TiO_2 phases, etc.) could be taken explicitly into account in the model formulations since they are believed to play an essential role on the effectiveness and would hence contribute to a significant reduction of the model uncertainties. However, this approach could only contribute to solving current needs and problems if material manufacturers would be legally required to furnish the authors of the decision analysis with required information on product characteristics. Where their products are patented, such disclosure should be subject to confidentiality agreements.

5. Conclusions

Based on *in situ*-measurements realised by means of the "PhotonSite" device, the present study addressed the revision of a statistical regression model for a comparative predictions of photocatalytic NO_x removal behaviour of different urban pavement materials under various environments. Such a model represents a significant step towards knowledge-based decisions concerning the choice of appropriate materials under specific circumstances. The strong parallels among experimental and modelling results obtained in the study lent support to the following conclusions:

- The exposure time *t* or ageing is the only statistically significant variable for explanation of the performance of photocatalytic emulsions coating asphalt substrates (E/A, type III). Microscopic observations confirmed this finding, showing that the emulsions are progressively removed from the substrate with increasing t, most likely due to loss of adherence.
- For type I (S/A) and type II (T), the most relevant explanatory variable corresponds to the relative air humidity over *X* days preceding the NO_x removal test, RH_X. This variable is a representative measure for the hygroscopic conditions of the substrate. The

optimum number of days considered for computation of RH_X should be in the range 3–7 days. Variable RH_X has a negative influence on the NO_x abatement effectiveness of the materials, i.e. the higher RH_X the lower R_{NOx}.

- In addition to RH_X, product-specific influences related to the quality of the photocatalytic layer on top of the substrate surface, in terms of continuity, homogeneity, compactness, thickness or adhesion, were found to have substantial influence on R_{NOx} of the S/A and T materials. Microscopic analysis of the samples validated this result by revealing significant differences in the quality of the photocatalytic layers on different materials.
- The exposure time *t* has certain influence on the NO_x abatement for type I and II materials, although to a far less extent, than for the type III materials. In addition to loss of adherence, microscopic observations could relate the time-dependant deterioration to formation of a calcite layer due to carbonation. This layer can block both the UV radiation and the access of NO_x to the TiO_2 active centres that leads to the effectiveness decrease.

Declaration of Competing Interest

The authors declare that they have no known competing financial interests or personal relationships that could have appeared to influence the work reported in this paper.

Acknowledgements

This study was funded by the LIFE Photoscaling program (LIFE 13/ENV/ES/001221, http://www.life-photoscaling.eu/). The authors are grateful to Luis Cordoba and Francisco Rubiano for their contribution in the experimental part.

References

[1] M.M. Ballari, M. Hunger, G. Hüsken, H. Brouwers, NOx photocatalytic degradation employing concrete pavement containing titanium dioxide, Appl. Catal. B 95 (3–4) (2010) 245–254.
[2] N. Bengtsson, M. Castellote, Photocatalytic activity for NO degradation by construction materials: parametric study and multivariable correlations, J. Adv. Oxidation Technol. 13 (3) (2010) 341–349.
[3] E. Boonen, A. Beeldens, Photocatalytic roads: From lab tests to real scale applications, Eur. Transport Res. Rev. 5 (2) (2013) 79–89, https://doi.org/10.1007/s12544-012-0085-6.
[4] E. Boonen, A. Beeldens, Recent photocatalytic applications for air purification in Belgium, Coatings 4 (3) (2014) 553–573.
[5] S. Caillol, Fighting global warming: the potential of photocatalysis against CO2, CH4, N2O, CFCs, tropospheric O3, BC and other major contributors to climate change, J. Photochem. Photobiol., C 12 (1) (2011) 1–19.
[6] Castellote, M. (2016). Device for determiming photocatalytic properties of materials. PCT/ES2016/070808.
[7] D.H. Chen, K. Li, R. Yuan, Photocatalytic coating on road pavements/structures for NOx abatement, Lamar Univ. Rep. (2007) 1–17.
[8] J. Chen, C.-S. Poon, Photocatalytic construction and building materials: From fundamentals to applications, Build. Environ. 44 (9) (2009) 1899–1906, https://doi.org/10.1016/j.buildenv.2009.01.002.
[9] M. Chen, J.-W. Chu, NOx photocatalytic degradation on active concrete road surface—from experiment to real-scale application, J. Cleaner Prod. 19 (11) (2011) 1266–1272.
[10] J. Cordero, R. Hingorani, E. Jimenez-Relinque, M. Grande, R. Borge, A. Narros, M. Castellote, NOx removal efficiency of urban photocatalytic pavements at pilot scale, Sci. Total Environ. 719 (2020) 137459, , https://doi.org/10.1016/j.scitotenv.2020.137459.
[11] J. de O.B. Lira, N. Padoin, V.J.P. Vilar, C. Soares, Photocatalytic NOx abatement: Mathematical modeling, CFD validation and reactor analysis, J. Hazard. Mater. 145–153 (2019), https://doi.org/10.1016/j.jhazmat.2018.07.009.
[12] H. Dylla, S. Asadi, M. Hassan, L.N. Mohammad, Evaluating photocatalytic asphalt pavement effectiveness in real-world environments through developing models: a statistical and kinetic study, Road Mater. Pavement Design 14 (sup2) (2013) 92–105.
[13] A. Folli, C. Pade, T.B. Hansen, T. De Marco, D.E. Macphee, TiO 2 photocatalysis in cementitious systems: insights into self-cleaning and depollution chemistry, Cem. Concr. Res. 42 (3) (2012) 539–548.
[14] M. Gallus, R. Ciuraru, F. Mothes, V. Akylas, F. Barmpas, A. Beeldens, J. Kleffmann, Photocatalytic abatement results from a model street canyon, Environ. Sci. Pollut. Res. 22 (22) (2015) 18185–18196, https://doi.org/10.1007/s11356-015-4926-4.
[15] C. George, A. Beeldens, F. Barmpas, J.F. Doussin, G. Manganelli, H. Herrmann, A. Mellouki, Impact of photocatalytic remediation of pollutants on urban air quality, Front. Environ. Sci. Eng. 10 (5) (2016), https://doi.org/10.1007/s11783-016-0834-1.
[16] M.J. Hernández-Rodríguez, R.S. Rodríguez, R. Darias, O.G. Díaz, J.M.P. Luzardo, J.M.D. Rodríguez, E.P. Melián, Effect of TiO2 addition on mortars: Characterization and photoactivity, Appl. Sci. (Switzerland) 9 (13) (2019), https://doi.org/10.3390/app9132598 http://www.life-photoscaling.eu/.
[18] E. Jimenez-Relinque, M. Castellote, Hydroxyl radical and free and shallowly trapped electron generation and electron/hole recombination rates in TiO2 photocatalysis using different combinations of anatase and rutile, Appl. Catal. A: Gen. (2018).
[19] E. Jimenez-Relinque, R. Hingorani, F. Rubiano, M. Grande, A. Castillo, M. Castellote, In situ evaluation of the NOx removal efficiency of photocatalytic pavements: statistical analysis of the relevance of exposure time and environmental variables, Environ. Sci. Pollut. Res. 26 (36) (2019) 36088–36095, https://doi.org/10.1007/s11356-019-04322-y.
[20] E. Jimenez-Relinque, J. Rodriguez-Garcia, A. Castillo, M. Castellote, Characteristics and efficiency of photocatalytic cementitious materials: Type of binder, roughness and microstructure, Cem. Concr. Res. 71 (2015) 124–131.
[21] A.M. Kaja, H.J.H. Brouwers, Q.L. Yu, NOx degradation by photocatalytic mortars: The underlying role of the CH and C-S-H carbonation, Cem. Concr. Res. 125 (2019), https://doi.org/10.1016/j.cemconres.2019.105805.
[22] J. Kleffmann, Discussion on “field study of air purification paving elements containing TiO2” by Folli et al. (2015), Atmos. Environ. 129 (2016) 95–97, https://doi.org/10.1016/j.atmosenv.2016.01.004.
[23] T. Maggos, A. Plassais, J. Bartzis, C. Vasilakos, N. Moussiopoulos, L. Bonafous, Photocatalytic degradation of NOx in a pilot street canyon configuration using TiO 2-mortar panels, Environ. Monit. Assess. 136 (1–3) (2008) 35–44.
[24] J. Mo, Y. Zhang, Q. Xu, J.J. Lamson, R. Zhao, Photocatalytic purification of volatile organic compounds in indoor air: a literature review, Atmos. Environ. 43 (14) (2009) 2229–2246.
[25] R. Nevshupa, M. Castellote, J.A.C. Cornelio, A. Toro, Triboemission of FINE and ultrafine aerosol particles: A new approach for measurement and accurate quantification, Lubricants 8 (2) (2020) 21 Retrieved from https://www.mdpi.com/2075-4442/8/2/21.
[26] I.G.D. Rocha Segundo, S. Landi Jr, S.M.B. Oliveira, E.F.D. Freitas, J.A.O. Carneiro, Photocatalytic asphalt mixtures: Mechanical performance and impacts of traffic and weathering abrasion on photocatalytic efficiency, Catal. Today 94–100 (2019), https://doi.org/10.1016/j.cattod.2018.07.012.
[27] J.K. Sikkema, S.K. Ong, J.E. Alleman, Photocatalytic concrete pavements: Laboratory investigation of NO oxidation rate under varied environmental conditions, Constr. Build. Mater. 100 (2015) 305–314, https://doi.org/10.1016/j.conbuildmat.2015.10.005.
[28] Smith, G. (1988). Statistical Reasoning (2 ed.): Allyn and Bacob, Inc.
[29] S. Suarez, R. Portela, M.D. Hernández-Alonso, B. Sánchez, Development of a versatile experimental setup for the evaluation of the photocatalytic properties of construction materials under realistic outdoor conditions, Environ. Sci. Pollut. Res. 21 (19) (2014) 11208–11217.
[30] Sullivan, T. (2020, February 18, 2020). Fuchs: China Sags, Sustainability Looms. Lubes'N'Grises. Lube report EMEA. Retrieved from https://pubs.lubesngreases.com/lubereport-emea/fuchs-china-sags-sustainability-looms/.
[31] Eva Jimenez-Relinque, Francisco Rubiano, Ramon Hingorani, Maria Grande, Angel Castillo, Roman Nevshupa, Marta Castellote, A New Holistic Conceptual Framework for Assessment of Photocatalytic Pavements Performance, Front. Chem. - Catal. Photocat. (2020) Submitted for publication.
[32] Roman Nevshupa, Eva Jimenez-Relinque, Maria Grande, Emilio Martinez, Marta Castellote, Assessment of urban air pollution related to potential nanoparticle emission from photocatalytic pavements, J. Environ. Manag. (2020), https://doi.org/10.1016/j.jenvman.2020.111059.
[33] Eva Jimenez-Relinque, Maria Grande, Teresa Duran, Angel Castillo, Marta Castellote, Environmental impact of nano-functionalized construction materials: leaching of titanium and nitrates from photocatalytic pavements under outdoor conditions, Sci. Total Environ. (2020), https://doi.org/10.1016/j.scitotenv.2020.140817 In press.